SIMULTANEOUS MEASURMENT OF FLUCTUATING VELOCITY AND PRESSURE USING TIME-RESOLVED PIV AND MINIATURE STATIC-PRESSURE PROBES

Takuya Kawata, Shinnosuke Obi
Department of mechanical engineering, Keio University
3-14-1 Hiyoshi, Kohoku-ku, Yokohama, Kanagawa 223-8522, Japan
slowhand@z7.keio.jp (T. Kawata)
obsn@mech.keio.ac.jp (S. Obi)

ABSTRACT

Simultaneous measurement of the fluctuating velocity and pressure is performed combining a miniature static-pressure probe and a time-resolved PIV aiming at further improvement in evaluation of the velocity-pressure correlation. Two static-pressure probes were placed in the measurement domain of the time-resolved PIV and the instantaneous velocity field and the fluctuating velocity are measured simultaneously. The instantaneous pressure filed is estimated from the measured velocity field by numerically solving a discrete Poisson equation for pressure. The values of the estimated pressure are corrected based on the pressure values which are directly measured by the static-pressure probe.

INTRODUCTION

The pressure-related turbulence statistics, such as the velocity-pressure correlation, the velocity pressure-gradient correlation, have been recognized as the important properties to understand the transport phenomena in complex turbulent flows associated with large-scale vortex structure. A number of efforts have been made for simultaneous measurement of fluctuating velocity and pressure to evaluate such pressure-related statistics. Following the pioneering development of a miniature-static pressure probe (SP - probe) by Toyoda *et al.* (1994), simultaneous measurement of velocity and pressure at single point using the SP-probe and a hot-wire probe was performed by several researchers including authors′ research group (e.g. Naka *et al.*, 2006; Tsuji *et al.*, 2007; Terashima *et al.*, 2012).

On the other hand, some attempts have been made to numerically estimate the instantaneous pressure field from the velocity data measured by a particle image velocimetry (PIV) (e.g. Obi & Tokai, 2006; Charonko *et al.*, 2010; De Kat & van Oudheusden, 2012). In this method, the velocity data measured by the PIV are substituted into the velocity terms in a Poisson equation of pressure, and the instantaneous pressure field is obtained as a numerical solution of the Poisson equation. This method has a great advantage that the instantaneous fields of both of velocity and pressure are obtained, while it still suffers from some problems such as influence of the noise included in velocity measurement by PIV on pressure estimation and specification of the boundary condition.

In the present study, the direct and sing-point measurement of fluctuating pressure by the SP-probe and the velocity measurement by a time-resolved PIV are performed simultaneously aiming at further improvement of the accuracy of the pressure estimation from the PIV data. The SP-probes were placed in the measurement domain of the time-resolved PIV, and the instantaneous velocity fields and the fluctuating static-pressure were measured simultaneously in a turbulent wake of a circular cylinder. The pressure values directly measured by the SP-probe are used to specify values of the estimated pressure field, and the validity is discussed.

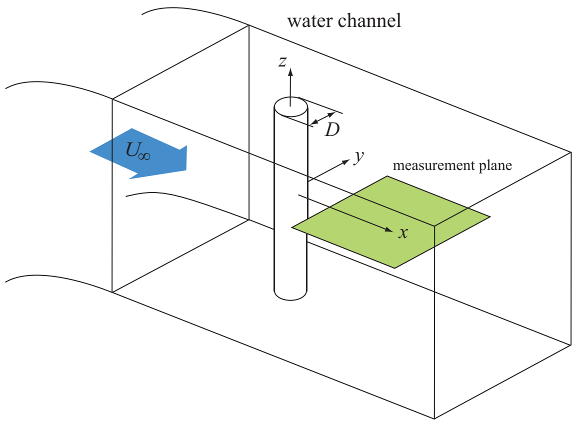

Figure 1. Schematics of test section.

EXPERIMENT

Flow System

The test section is schematically shown in Fig. 1. The measurements were undertaken in a closed-loop water channel with the free stream velocity U_∞ being 280 mm/s. A circular cylinder was placed in the free stream, and the diameter D was 20 mm. The origin of Cartesian coordinates was fixed at the trailing edge of the tip, and x, y and z axes were taken in streamwise, transversewise and spanwise direction. The domain measured in the present study was the near region of the cylinder wake, $0.6D \leq x \leq 4.52D$, $-2.12D \leq y \leq 1.88D$. The temperature of the water was 24.6° during the experiment and the Reynolds number based on D and U_∞ was $\mathrm{Re} = 7800$.

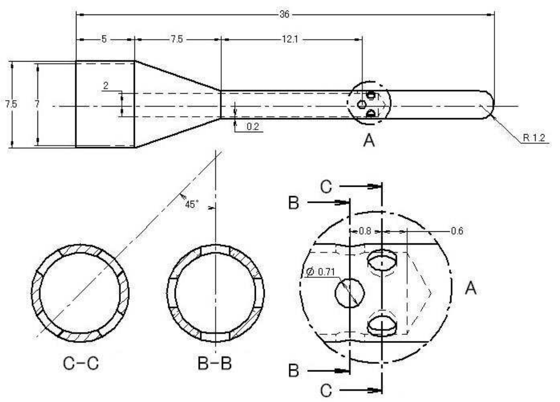

Figure 2. Static-pressure probe.

Fluctuating Pressure Measurement

The SP-probe employed for direct measurement of the fluctuating pressure is schematically shown in Fig. 2. The SP-probe was made of transparent material and consisted of a thin pipe with a circular-rounded tip. The outer diameter and the thickness of the pipe were 2.4 mm and 0.4 mm, respectively. Eight small pressure-sensing holes with the diameter of 0.71 mm were placed on the surface of the pipe. For the fluctuating pressure measurement, the SP-probe is connected to the main port of a pressure transducer (DP-45, Validyne) placed out of the water tunnel by a tube as shown in Fig. 5. The SP-probe, the tube and the cavity in the pressure transducer were filled with water. The pressure transducer was operated in the differential mode, and the reference port was opened to the atmosphere.

Due to the elasticity of the diaphragm of the pressure transducer and the viscosity of the fluid in the thin pipe of the SP-probe, the pressure-measuring system which consists of the SP-probe, the tube and the pressure transducer has non-flat frequency response. The dynamic response of such system has been investigated (e.g. Donovan *et al.*, 1991), the relationship between the true fluctuating-pressure p_s and the measured pressure p_m are modeled as

$$\frac{d^2 p_m}{dt^2} + 2\omega_n \xi \frac{d p_m}{dt} + \omega_n^2 p_n = \omega_n^2 p_s, \qquad (1)$$

where ξ and ω_n are the damping factor and the resonance angular velocity of the system, respectively. The amplitude ratio A and the phase delay $\Delta\theta$ between p_m and p_s are

$$A = \frac{1}{\sqrt{(1-\beta^2)^2 + 4\xi^2\beta^2}}, \qquad (2)$$

$$\Delta\theta = \tan^{-1}\left(\frac{2\xi\beta}{1-\beta^2}\right), \qquad (3)$$

where β is the frequency of the fluctuating pressure scaled by ω_n.

Figure 3 shows a schematics of the system of dynamic calibration of the pressure-measuring system. Two pressure transducers; the main port of the main pressure transducer was connected to the SP-probe placed in the water channel, and the other is outside of the channel and the main port is opened to the atmosphere. The reference ports of the pressure transducers were connected to the pressure chamber,

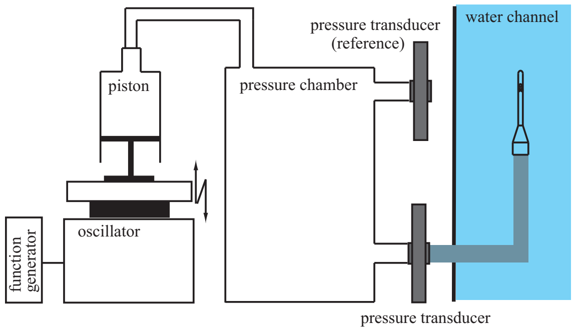

Figure 3. Calibration of dynamic response of pressure-measuring system.

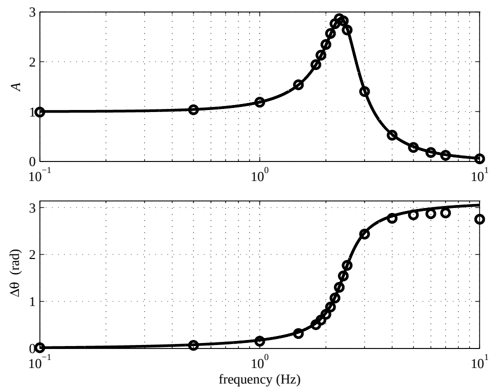

Figure 4. Dynamic response of pressure-measuring system; circle plot, measured values; solid line, profile fitted to Eq. (2) and (3).

in which the pressure was variable by a piston. Sinusoidal input of pressure variation was generated by an oscillator controlled by a function generator. The pressure variation was measured by the two pressure transducer, amplitude ratio A and the phase delay $\Delta\theta$ were obtained by comparing the pressure signals. The variation of A and $\Delta\theta$ measured in the calibration are shown in Fig. 4. The resonance angular velocity ω_n and the damping factor ξ was evaluated by Eq. (2) and (3) to measured values of A and $\Delta theta$ as $\omega_n = 15.2$ and $\xi = 0.177$. The dynamic response of the pressure-measuring system shows the peak of A by resonance at 2.3 Hz and the significant phase in the frequency range higher than 2 Hz.

Instruments and Data Acquisition

The system for the simultaneous measurement of velocity and pressure is shown in Fig. 5 Three SP-probes were placed in a wake of the circular cylinder. The SP-probe 1 and 2 were fixed in the measurement domain of the PIV, at $x_1 = (4.3D, 1.6D)$ and $x_2 = (4.3D, -2.1D)$, respectively, and the third SP-probe was placed at the same streamwise location but outside of the wake for reduction of the background noise which was conducted in the same manner as Naka *et al.* (2006). The SP-probes were fixed 10 mm below the laser sheet to avoid reflection of the laser. Based on the frequency response measured in the dynamic calibration, the pressure fluctuation in the frequency range higher than 4 Hz were filtered out and the amplitude and the phase

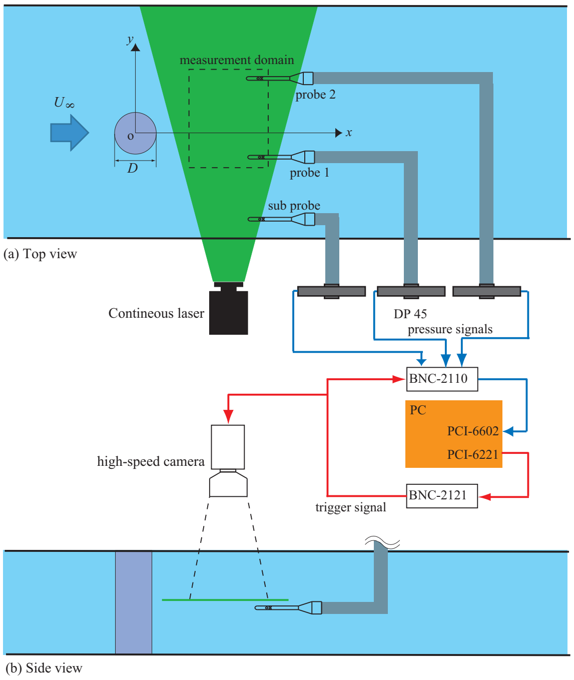

Figure 5. System of simultaneous measurement of velocity and pressure.

of those in the lower frequency range were corrected in the post processing.

The PIV measurement was undertaken by a time-resolved PIV system comprising a high-speed camera (FASTCAM SA3 model, Photron) with a 85 mm lens (Nikkor 85 mm f2.8D, Nikkon) and a continuous laser (LYPE2-SG-WL532CW LYPE). The resolution of the high-speed camera was 1024×1024 pixel^2, and White Nylon 12 particles, whose the mean diameter and the specific gravity were 90 μm and 1.02, respectively, were used as a tracer. The size of the interrogation area was 20×20 pixel^2, corresponding to 1.63×1.63 mm^2. The frame rate of the measurement was 1000 fps.

The image acquisition of the time-resolved PIV and the fluctuating pressure measurement by the SP-probes were synchronized by a trigger signal created by the operating PC. Receiving the trigger signal, the high-speed camera started the PIV measurement. The trigger signal was recorded with the pressure signals from the pressure transducer with the sampling rate of 10 kHz, and the pressure values which were acquired simultaneously with the velocity measurement by the PIV were extracted from the measured time-series of the pressure signals by the raising edge of the trigger signal.

Estimation of Instantaneous Pressure Field from PIV Data

The instantaneous pressure field was evaluated from the PIV data in the same manner used in Obi and TokaiObi & Tokai (2006). Assuming that the spanwise velocity-gradient is sufficiently small, the Poisson equation for the pressure of the incompressible flow is approximated into two-dimensional form as

$$\frac{\partial^2 p}{\partial x^2}+\frac{\partial^2 p}{\partial y^2}=2\rho\left(\frac{\partial u}{\partial x}\frac{\partial v}{\partial y}-\frac{\partial u}{\partial y}\frac{\partial v}{\partial x}\right) \tag{4}$$

where u and v are the velocity components in $x-$ and $y-$direction.

For the Neumann condition for Eq. (4), the spatial gradient of the pressure normal to the boundaries was evaluated using the 2D-approximated Euler′s equation,

$$\frac{\partial p}{\partial n}=-\left(\frac{\partial \rho u_n}{\partial t}+u_n\frac{\partial \rho u_n}{\partial n}+u_s\frac{\partial u_n}{\partial s}\right) \tag{5}$$

with n and s being the normal and tangential direction of the boundary, respectively.

The numerical solution of Eq. (4) was obtained by means of a finite-volume-method. Denoting by P the node at which Eq. (4) is discretized and those surrounding it by E, S, W and N, a discrete form of Eq. (4) is

$$\frac{\Delta y}{\Delta x}(p_{\mathrm{E}}+p_{\mathrm{W}})+\frac{\Delta x}{\Delta y}(p_{\mathrm{N}}+p_{\mathrm{S}})-2\left(\frac{\Delta y}{\Delta x}+\frac{\Delta x}{\Delta y}\right)p_{\mathrm{P}}=S \tag{6}$$

with Δx and Δy being the grid spacing in $x-$ and $y-$, and S being the source term from the right-hand-side of Eq. (4):

$$S=2\rho\left(\frac{\partial u}{\partial x}\frac{\partial v}{\partial y}-\frac{\partial u}{\partial y}\frac{\partial v}{\partial x}\right)\Delta x\Delta y \tag{7}$$

The contents of S were calculated by differentiating the PIV data. Equation (4) was solved using the iterative solver "`lsqr`" available in MATLAB ® with the tolerance of 10^{-3}.

RESULTS AND DISCUSSION

The instantaneous velocity field measured by the time-resolved PIV is presented in Fig. 6. The color shows the magnitude of the velocity vector $\sqrt{u^2+v^2}$ scaled by the free stream velocity U_∞, and the black arrows indicate the direction. Figure 7 presents the instantaneous pressure field obtained from the instantaneous velocity field shown in Fig. 6 by solving Eq. (4). The values of pressure are scaled by ρU_∞^2. The black arrows indicates a helical motion of the fluid by the vortex shed from the cylinder around $(x,y)=(1.2D,-0.25D)$, and the minimum of the pressure locates near the center of the vortex. Additionally, Figure 7 shows a high-pressure region and a low-pressure region around $(x,y)=(4.0D,0.5D)$ and $(4.4D,0.45D)$, corresponding to a low-speed region and a high-speed region shown in Fig. 6, respectively.

To verify the estimation of the instantaneous pressure field, the acceleration of the fluid and the pressure gradient are compared. Since the Reynolds number is sufficiently large, the acceleration of the fluid should show the similar distribution to the pressure gradient:

$$a_x=\frac{Du}{Dt}=\frac{\partial u}{\partial t}+u\frac{\partial u}{\partial x}+v\frac{\partial u}{\partial y}\simeq-\frac{1}{\rho}\frac{\partial p}{\partial x} \tag{8}$$

$$a_y=\frac{Dv}{Dt}=\frac{\partial v}{\partial t}+u\frac{\partial v}{\partial x}+v\frac{\partial v}{\partial y}\simeq-\frac{1}{\rho}\frac{\partial p}{\partial y} \tag{9}$$

In Fig. 8 the pressure gradient $-\partial p/\partial x$ obtained from the instantaneous pressure field shown in Fig. 7 is compared with the streamwise acceleration a_x evaluated by Eq. (8).

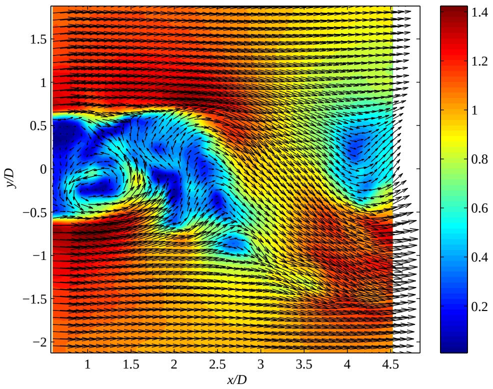

Figure 6. Instantaneous velocity field measured by the time-resolved PIV.

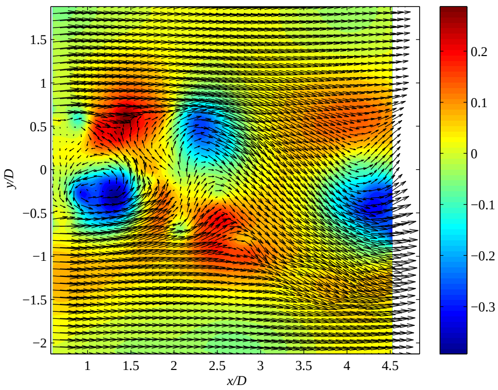

Figure 7. Instantaneous pressure field estimated from PIV data shown in Fig. 6

The a_x is more jaggy distribution compared to the pressure gradient, but the pattern of the sign is roughly similar. The correlation coefficient between a_x and $-\partial p/\partial x$ and between a_y and $-\partial p/\partial y$ are 0.41 and 0.42, respectively.

Figure 9 shows the r.m.s. values of the pressure fluctuation p' estimated from the time-resolved PIV data with the streamlines calculated from the average velocity. To specify the pressure values, the values of instantaneous pressure at $(x,y) = (0.6D, -2.1D)$ are fixed to zero. It is shown that two significant peak of p' locates on the outer edge of the recirculation region. On the downstream-side boundary of the domain, $x = 4.52D, -1D \leq y \leq 1D$, and on the domain corner, $(x,y) = (-0.6D, 1.88D), (4.52D, 1.88D)$, increase of the pressure fluctuation is observed, which may be attributable to numerical problems in implementation of the boundary condition. The location of the SP-probes are indicated by the red circles in Fig. 9, and the probe 1 is located near $(x,y) = (4.52D, 1.88D)$, and the estimated pressure at x_1 might be influenced.

The profiles of the mean pressure P and the pressure fluctuation p' at $x = 3D$ were also directly measured by the SP-probe. Figure 10 compares the measured profiles with those estimated from the PIV data. The distribution of P directly measured by SPP shows the pressure minimum at the wake center, while the results obtained from PIV has two maxima beside the wake center and the pressure loss at the wake center is smaller than that by the SP-probe. The profile of p' shows two peaks beside the wake center and

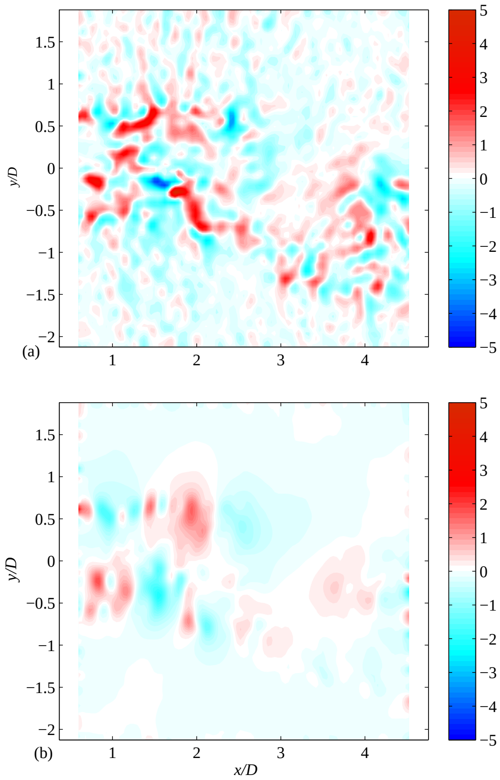

Figure 8. instantaneous distribution of streamwise acceleration and streamwise pressure gradient: (a), streamwise acceleration a_x; (b), pressure gradient $-\partial p/\partial x$.

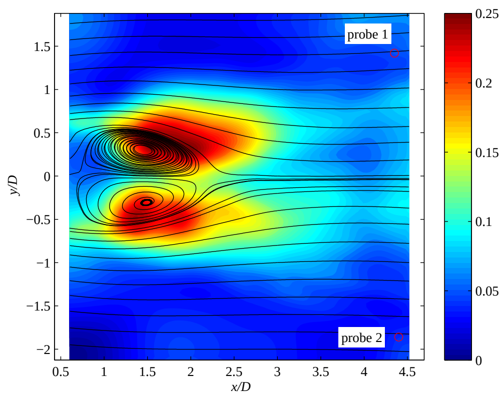

Figure 9. Distribution of pressure fluctuation p' estimated from PIV data.

the directly measured profile and the estimated profile are in quite good agreement.

Figure 11 shows the time history of the fluctuating pressure at $(x,y) = x_2$ and x_1, comparing those estimated from the PIV data and directly measured by the SP-probes. In Fig. 11a, it is indicated that both of the estimated and measured pressure signal show periodic time history and the amplitude of the fluctuation are in the same order with each other However, there is still certain time lag between the estimated and measured pressure signals, and the correlation coefficients between them are 0.049.

The estimated pressure at $(x,y) = x_1$ is corrected using

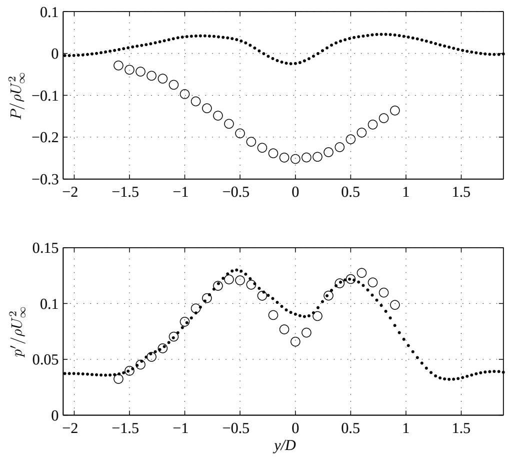

Figure 10. Distribution of mean pressure P and pressure fluctuation p' at $x = 3D$; dots, estimated pressure from PIV data; circle, directly measured pressure by SP-probe.

the values of the fluctuating pressure at $(x, y) = x_2$ as:

$$p_{\text{est,corr}}(x_1) = p_{\text{est}}(x_1) - (p_{\text{est}}(x_2) - p_{\text{meas}}(x_2)) \qquad (10)$$

where p_{est} and p_{meas} stand for the fluctuating pressure estimated from the PIV data and that directly measured by the SP-probe, respectively. The time history of the estimated pressure, estimated and corrected pressure and directly measured pressure at x_1 are compared in Fig. 11b. The signals of $p_{\text{est}}(x_1)$, $p_{\text{est,corr}}(x_1)$ shows the fluctuation of same order with $p_{\text{meas}}(x_1)$, but there are still phase lag between the estimated and measured time-history of the fluctuating pressure. The correlation coefficient between $p_{\text{est}}(x_1)$, $p_{\text{est,corr}}(x_1)$ and $p_{\text{meas}}(x_1)$ are 0.095 and -0.36, respectively.

The power spectra of $p_{\text{est,corr}}(x_1)$, $p_{\text{est}}(x_1)$ and $p_{\text{meas}}(x_1)$ are compared in Fig. 12a. The PSD of the measured pressure fluctuation shows a significant peak at $f = 0.17U_\infty/D$, which is corresponding to the vortex shedding frequency, and in the frequency range of $fD/U_\infty \leq 0.3$, the PSD rapidly decreases due to the filtering. The PSDs of estimated fluctuating pressure also show the peak at the vortex shedding frequency and the peak magnitude is in good agreement with that of the measured PSD, indicating that the pressure fluctuation due to the vortex shedding is captured by the estimation of the pressure field from the PIV data.

The cross-correlation coefficients with the measured pressure signals at $(x, y) = x_1$ defined as

$$C_a(\Delta t) = \frac{\overline{a(t)p_{\text{meas}}(t+\Delta t)}}{\sqrt{\overline{a^2}}\sqrt{\overline{p_{\text{meas}}^2}}} \qquad (11)$$

are plotted in Fig. 12b. The cross-correlation coefficient $C_{p_{\text{est,corr}}}$ and $C_{p_{\text{est}}}$ are -0.36 and 0.095, respectively, at $\Delta t = 0$ ms as mentioned above. Comparing the profiles of the cross-correlations, the maximum value of the correlation slightly increases form 0.43 ($C_{p_{\text{est}}}$) to 0.59 ($C_{p_{\text{est,corr}}}$) and the location of the maximum also changes from $\Delta t = 0.09$ s

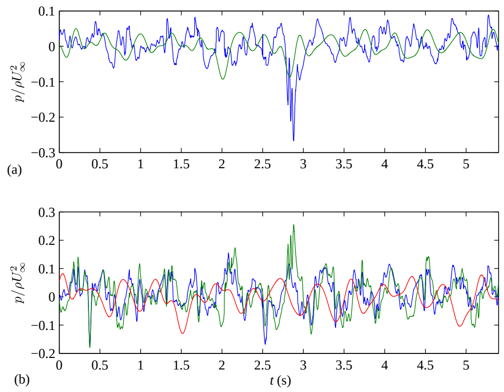

Figure 11. Time history of fluctuating pressure. (a): at x_2; blue, estimated from PIV data; green, measured by SP-probe 2. (b): at x_1; blue, estimated from PIV data; green, estimated from PIV data, corrected; red, measured by SP-probe 1

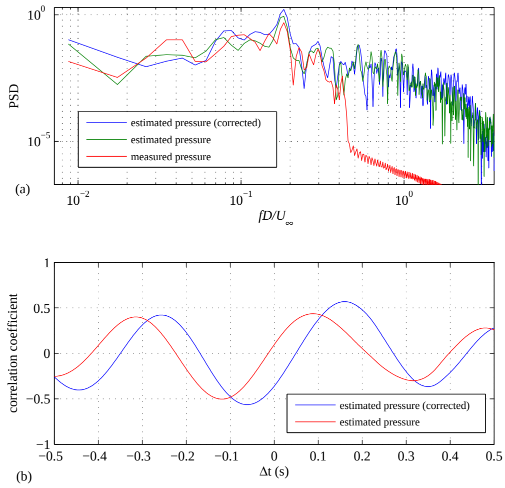

Figure 12. Power spectrum density and cross correlation of pressure fluctuation at x_1; (a) power spectra of fluctuating pressures; (b) cross correlation between the estimated pressure and the measured pressure.

($C_{p_{\text{est}}}$) to $\Delta t = 0.16$ s ($C_{p_{\text{est}},corr}$). It is indicated that by the correction based on the measured pressure signals at $(x, y) = x_2$, the time history of the estimated pressure at $(x, y) = x_1$ was delayed by 0.07 s, corresponding to 77° of the vortex shedding period and the correlation between the estimated and directly measured pressure was not improved.

The velocity-pressure correlation $\overline{up}$ obtained from the velocity and pressure fields obtained by the PIV measurement is shown in Fig. 13. In evaluation of $\overline{up}$, the pressure field is corrected in the same manner as Eq. (10), and the values of $\overline{up}$ are scaled by ρU_∞^3. The velocity-pressure correlation $\overline{up}$ shows two significant negative minima at the locations corresponding to the peak locations of the pressure fluctuation shown in Fig. 9. The probe position, $(x, y) = x_1$ and x_2, are indicated by the circles in the figure, again, and the correlation coefficient $\overline{up}/u_{\text{rms}}p_{\text{u}}$ at $(x, y) = x_1$ is 0.511. However, in our previous study(Kawata *et al.*, 2011), the $\overline{up}$ showed negative values in wide range across the wake. The correlation coefficient between the streamwise velocity and

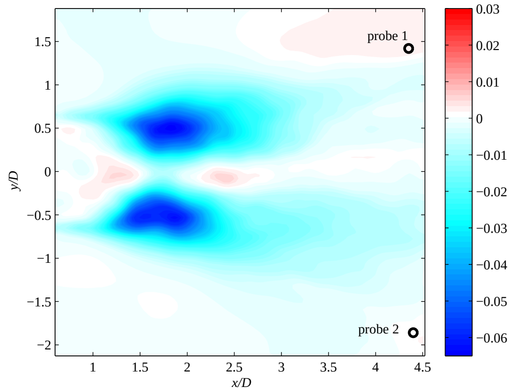

Figure 13. Distribution of velocity-pressure correlation $\overline{up}$.

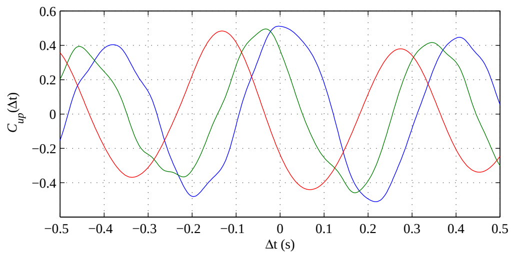

Figure 14. Cross-correlation between streamwise velocity and fluctuating pressure; blue, estimated and corrected pressure; green, estimated pressure; red, measured pressure.

the pressure measured at $(x,y) = x_1$ is -0.236.

The velocity-pressure cross-correlation coefficient at $(x,y) = x_1$ are shown in Fig. 14, comparing those between the streamwise velocity measured by the PIV and the estimated and corrected pressure $C_{up_{\mathrm{est,corr}}}$, the estimated and not corrected pressure $C_{up_{\mathrm{est}}}$ and the measured pressure $C_{up_{\mathrm{meas}}}$. As mentioned above, the cross-correlation coefficient $C_{up_{\mathrm{est,corr}}}$ and $C_{up_{\mathrm{meas}}}$ are 0.511 and -0.236, respectively, at $\Delta t = 0$ s, and $C_{up_{\mathrm{est}}}$ is 0.372 at $\Delta t = 0$ s. It is shown that the variation of at $C_{up_{\mathrm{est,corr}}}$ is shifted by about -0.06 s compared to the profile of $C_{up_{\mathrm{est}}}$ and the profile of $C_{up_{\mathrm{est,corr}}}$ is in antiphase of that of $C_{up_{\mathrm{meas}}}$, which is consistent with the cross correlation between the pressure signals shown in Fig. 12.

Certain disagreement between the estimated pressure and the measured pressure has been observed although it is confirmed that the typical frequency and the magnitude of the pressure fluctuation were captured by the pressure estimation from the PIV data. The disagreement might be attributed to the pressure fluctuation which numerically took place near the boundary. Further improvement is necessary for the agreement between the velocity-pressure correlation based on the measured pressure and the estimated pressure.

CONCLUDING REMARKS

In the present study, simultaneous measurement of fluctuating velocity and pressure was conducted combining velocity measurement by time-resolved PIV and fluctuating pressure measurement by static-pressure probe. The fluctuating pressure was directly measured at two points in the measurement domain of the time-resolved PIV simultaneously with the velocity measurement. The instantaneous pressure field was numerically estimated from the instantaneous velocity field measured by the PIV and the pressure values directly measured by the static-pressure probe were used for correction and comparison. The estimation of fluctuating pressure from the PIV data captured the typical frequency and the amplitude of the fluctuation associated with the vortex shedding from the circular cylinder, although certain disagreement between the measured and estimated pressure is still remained. The disagreement between the measured and estimated pressure might be attributed to the pressure fluctuation which numerically took place near the boundary of the domain.

REFERENCES

Charonko, J. J., King, C. V., Smith, B. L. & Vlachos, P. P. 2010 Assesment of pressure fieldscalculations from particle image velocimetry measurement. *Meas. Sci. Technol.* **21**, 105401 (15pp).

De Kat, R. & van Oudheusden, B. W. 2012 Instantaneous planar pressure determination from PIV in turbulent flow. *Exp. Fluids* **52–5**, 1089–1106.

Donovan, F. M., Taylor, B. C. & Su, M. C. 1991 one-dimensional computer analysis of oscillatory flow in rigid tubes. *Trans. ASME J. Biomech. Eng.* **113**, 476–484.

Kawata, T., Naka, Y., Fukagata, K. & Obi, S. 2011 Velocity-pressure correlation measurement using various static-pressure probes in a wake of a ciruclar cylinder. In *Proc: 7th International Symposium on Turbulent Shear Flow Phenomena*.

Naka, Y., Omori, T., Obi, S. & Masuda, S. 2006 Simultaneous measurement of fluctuating velocity and pressure in a turbulent mixing layer. *Int. J. Heat Fluid Flow* **27**, 737–746.

Obi, S. & Tokai, N. 2006 The pressure-velocity correlation in oscillatory turbulent flow between a pair of bluff bodies. *Int. J. Heat Fluid Flow* **27**, 768–776.

Terashima, O., Sakai, Y. & Nagata, K. 2012 Simultaneous measurement of velocity and pressure in a plane jet. *Exp. Fluids* **53–4**, 1149–1164.

Toyoda, K., Okamoto, T. & Shirahama, Y. 1994 Eduction of vortical structures by pressure measurements in noncircular jets. *Applied Scientific Research* **53**, 273–248.

Tsuji, Y., Fransson, J. H. M., Alfredsson, P. H. & Johansson, A. V. 2007 Pressure statistics and their scaling in high-Reynolds-number turbulent boundary layers. *J. Fluid Mech.* **585**, 1–40.